

ON THE X-RAY OUTBURSTS OF TRANSIENT ANOMALOUS X-RAY PULSARS AND SOFT GAMMA-RAY REPEATERS

ŞİRİN ÇALIŞKAN AND ÜNAL ERTAN

Sabancı University, Orhanlı-Tuzla, İstanbul, 34956, Turkey

Received 2012 February 16; accepted 2012 September 4; published 2012 October 4

ABSTRACT

We show that the X-ray outburst light curves of four transient anomalous X-ray pulsars (AXPs) and soft gamma-ray repeaters (SGRs), namely, XTE J1810–197, SGR 0501+4516, SGR 1627–41, and CXOU J164710.2–455216, can be produced by the fallback disk model that was also applied to the outburst light curves of persistent AXPs and SGRs in our earlier work. The model solves the diffusion equation for the relaxation of a disk that has been pushed back by a soft gamma-ray burst. The sets of main disk parameters used for these transient sources are very similar to each other and to those employed in our earlier models of persistent AXPs and SGRs. There is a characteristic difference between the X-ray outburst light curves of transient and persistent sources. This can be explained by the differences in the disk surface density profiles of the transient and persistent sources in quiescence indicated by their quiescent X-ray luminosities. Our results imply that a viscous disk instability operating at a critical temperature in the range of $\sim 1300\text{--}2800$ K is a common property of all fallback disks around AXPs and SGRs. The effect of the instability is more pronounced and starts earlier for the sources with lower quiescent luminosities, which leads to the observable differences in the X-ray enhancement light curves of transient and persistent sources. A single active disk model with the same basic disk parameters can account for the enhancement phases of both transient and persistent AXPs and SGRs. We also present a detailed parameter study to show the effects of disk parameters on the evolution of the X-ray luminosity of AXPs and SGRs in the X-ray enhancement phases.

Key words: accretion, accretion disks – pulsars: individual (AXPs) – stars: neutron – X-rays: bursts

1. INTRODUCTION

Anomalous X-ray pulsars (AXPs) and soft gamma-ray repeaters (SGRs) are a special population of young neutron stars whose rotational powers are not sufficient to account for their X-ray luminosities ($10^{34}\text{--}10^{36}$ erg s $^{-1}$; see Mereghetti 2008 for a recent review of AXPs and SGRs). The spin periods of all known AXP and SGRs are in the range of 2–12 s. These sources undergo short (< 1 s), super-Eddington soft gamma-ray bursts. Three out of four SGRs showed giant bursts with energies greater than 10^{44} erg. After a soft gamma-ray burst episode (it is likely that some of these bursts were missed), these sources enter an X-ray outburst/enhancement phase characterized by a sharp increase and eventual decay in X-ray luminosity. Some of the AXPs and SGRs have very low X-ray luminosities ($\sim 10^{33}$ erg s $^{-1}$) in the quiescent phase and were detected during these X-ray enhancement phases. These sources are called transient AXPs. During an outburst, X-ray luminosity, L_X , of the transient sources increases from a quiescent level of $\sim 10^{33}$ erg s $^{-1}$ to a maximum that remains in the L_X range of persistent AXP/SGRs ($10^{34}\text{--}10^{36}$ erg s $^{-1}$).

Energetics and timescales of the soft gamma-ray bursts, which are very likely to have magnetic origin, resulted in the classification of such objects as “magnetars” (Duncan & Thompson 1992). In the magnetar model, the source of the X-ray luminosity is the magnetic field decay, and the rotation rate of the neutron stars in these systems is assumed to be slowing down by the magnetic dipole torques in vacuum. This requires that the dipole component of the magnetic field has magnetar strength ($B_0 > 10^{14}$ G) on the surface of the neutron star. The magnetar model has no explanation for the period clustering of AXP/SGRs. Explaining the optical and infrared (IR) observations of persistent and transient AXP/SGRs in quiescent and outburst (enhancement) phases within the magnetar model also poses problems.

The fallback disk model (Chatterjee et al. 2000; Alpar 2001) was initially proposed to explain the spin periods and X-ray luminosities of AXPs and SGRs. It was suggested that the initial properties of fallback disks, together with magnetic dipole moment and initial spin period, could be responsible for the formation of the other young neutron star populations as well (Alpar 2001). Later, it was shown that the optical, IR, and X-ray observations of persistent AXPs and SGRs (hereafter, we use “AXPs” to denote both AXPs and SGRs) in both quiescent and enhancement phases can be explained consistently by the presence of active, accreting fallback disks in these systems (Ekşi & Alpar 2003; Ertan & Alpar 2003; Ertan & Cheng 2004; Ertan et al. 2006; Ertan & Çalışkan 2006). The detection of AXP 4U 0142+61 in mid-IR bands clearly indicates the presence of a disk around this source (Wang et al. 2006). These mid-IR data, together with earlier detections in optical and near IR bands, can be well fit by an irradiated active disk model, provided that the dipole field that interacts with the accretion disk has conventional values of $B_0 \simeq 10^{12}\text{--}10^{13}$ G on the surface of the young neutron star (Ertan et al. 2007). Coherently with these results, X-ray luminosity, period, period derivative, and statistical distribution of AXPs can also be produced by the evolution of the neutron stars with fallback disks and with dipole fields $B_0 < 10^{13}$ G (Ertan et al. 2009). Based on these constraints on B_0 indicated by our results, we proposed that the strong magnetic fields of AXPs must thus reside in multipoles that die rapidly in strength with increasing distance from the neutron star (Ekşi & Alpar 2003; Ertan et al. 2007, 2009). A recently reported upper bound on the period derivative of SGR 0418+5729 unambiguously revealed that the dipole field strength of this source cannot be greater than $\sim 7 \times 10^{12}$ G on the surface of the neutron star (Rea et al. 2010). This is in full agreement with our explanation and clearly shows that the soft gamma-ray bursts do not require magnetar dipole fields. Furthermore, if the dipole field is below this upper limit, then

the dipole spin-down age would not be accurate and other torque and magnetic field effects would need to be taken into account. In the frame of the disk model, rotational properties and X-ray luminosity of this SGR can be reached simultaneously within the cooling timescale of a neutron star with $B_0 \simeq 10^{12}$ G (Alpar et al. 2011). Recently, Trümper et al. (2010) showed that the high-energy spectrum of AXP 4U 0142+61 can be produced in the accretion column of this source mainly by the bulk Comptonization process.

In the present work, we investigate the X-ray enhancement (outburst) light curves of persistent and transient AXPs. We pursue the results of the work by Ertan & Erkut (2008) on the X-ray outburst light curve and the spin evolution of the transient AXP XTE J1810–197. The X-ray outburst light curve of this source showed a different decay morphology than those of persistent sources (Ibrahim et al. 2004; Bernardini et al. 2009). By means of model fits to the X-ray enhancement data, Ertan & Erkut (2008) concluded that this difference could be due to a viscous disk instability (see, e.g., Lasota 2001 for a review of the disk instability model (DIM)) in the fallback disks at a critical temperature in the ~ 1000 – 2000 K range. The fallback disks around AXPs are expected to have similar chemical compositions. If one of the AXP disks undergoes a thermal-viscous disk instability at a particular critical temperature, then the others are also expected to show the same instability at the same temperature. Our aim is to test this idea by applying the same model to the X-ray outburst data of other transient AXPs.

There are some difficulties in testing our model when the observed X-ray luminosity is close to the quiescent level ($L_X \sim 10^{33}$ erg s $^{-1}$) of the transient AXPs. As L_X decreases, temperature also decreases and thus effects of interstellar absorption increase. Furthermore, at these low temperatures, a significant fraction of the X-ray emission may come from outside the observational X-ray band and estimates of the bolometric luminosities are model dependent (Gotthelf & Halpern 2007; Bernardini et al. 2009). Our model gives the total accretion luminosity without addressing the X-ray spectrum from the surface or the accretion column of the neutron star. For comparison with data, we assume that the observed L_X is a close representation of the total L_X , which is a good assumption for the X-ray luminosities down to a few times 10^{33} erg s $^{-1}$ but does not allow a reliable comparison for lower luminosities. Another difficulty at very low L_X arises due to the fact that the luminosity contribution from the intrinsic cooling of the neutron star (Page et al. 2006) could become comparable to the accretion luminosity depending on the age of the source. Keeping these uncertainties in mind, we extend the model curves to the quiescent luminosity levels to present the model predictions at low L_X . As in other works on disk accretion, we do not perform χ^2 tests, since it is misleading due to the uncertainties in the disk, like the local instabilities close to the inner disk, that are not possible to address in the models.

Basic disk parameters, namely, the critical disk temperature, kinematic viscosity parameters, irradiation strength, and the radius dependence of the surface density of the extended disk, are expected to be similar in the fallback disks of different AXPs. This forces us to a difficult task of producing the X-ray outburst light curves of AXPs with a single set of these basic parameters. We describe our model and discuss the effect of the disk parameters on the X-ray luminosity evolution in Section 2. Properties of the transient AXPs that were observed in X-ray enhancement phases are summarized in Section 3. We discuss

the results of the model calculations in Section 4 and summarize our conclusions in Section 5.

2. THE NUMERICAL MODEL

2.1. Description of the Model Parameters

We solve the disk diffusion equation (see, e.g., Frank et al. 2002) in the way described in Ertan & Alpar (2003) and Ertan & Erkut (2008). In this model, it is assumed that a soft gamma-ray burst triggered on the surface of the neutron star pushes the inner disk matter outward. Some of this matter could escape from the system, while the remaining part creates a surface density gradient at the innermost disk. The resultant pileup, centered at r_0 , and the underlying disk distribution are represented by a Gaussian $\Sigma = \Sigma_{\max} \exp[-(r - r_0)^2/\Delta r^2]$ and a power-law $\Sigma = \Sigma_0(r_{\text{in}}/r)^p$ surface density profile, respectively, as the initial condition of the model.

We assume that the surface density profile of the innermost disk in the quiescent state is close to the standard thin disk profile $\Sigma \propto r^{-3/4}$, and the disk matter from r_{in} to a radius r_1 , with mass δM , is initially pushed out to a narrow radial region at radius r_1 by the burst. As the matter with a range of specific angular momentum mixes and piles up at r_1 , the angular momentum is redistributed rapidly due to mixing and the narrow radial extent of the pileup. The required timescale for the sharing of angular momentum is of the order of a few h/v_K , where v_K is the Keplerian velocity close to r_1 and h is the thickness of the disk, typical lengthscale for efficient viscous interaction, at r_1 . Taking $h(r_1) \sim 10^{-2}r_1$ and $r_1 \sim 10^{10}$ cm, $h/v_K \simeq 10^{-2}\Omega_K^{-1}$ is found to be a fraction of a second. This implies that the angular momentum is effectively shared during the formation of the pileup. After the burst episode, this matter circularizes at a radius between r_{in} and r_1 depending on the mean specific angular momentum of the pileup. The matter spreading from this circularization radius to both inner and outer radii with a surface density peak close to the circularization radius is represented by a Gaussian as the initial mass distribution in our model. The center r_0 of the Gaussian in the model could be assumed to represent this circularization radius.

Our model light curves do not sensitively depend on r_0 or the details of the Gaussian distribution. Similar model light curves could be produced with different r_0 values (within a factor of a few), provided that δM contained in the Gaussian distribution remains the same. This density gradient leads to an abrupt rise in the mass-flow rate at the innermost disk. The rise phase of the X-ray light curve is produced by the enhanced mass-flow rate to the Alfvén radius and subsequently onto the surface of the neutron star. Since the exact position of the inner disk radius, r_{in} , does not change the rate of mass inflow, for simplicity we take r_{in} constant and equal to the inner disk radius in quiescence. The mass accretion rate in the decay phase of the light curve is governed by the viscous relaxation of the inner disk matter. At the end of the decay phase, the luminosity converges to the quiescent X-ray luminosity level of the source. The X-ray luminosity produced by the inner disk through viscous dissipation is negligible compared to the luminosity powered by mass accretion onto the surface of the neutron star.

The evolution of the disk is determined by solving the diffusion equation (see, e.g., Frank et al. 2002). While δM is important in the evolution of the X-ray luminosity, the detailed shape of the Gaussian does not significantly affect the model light curve in the long term (Ertan et al. 2006). For a viscously evolving disk, the power index p of the extended surface density

profile is expected to be $\sim 3/4$ (Frank et al. 2002); we take $p = 3/4$ in our calculations.

We keep the inner radius of the disk r_{in} constant at a value near the Alfvén radius for a dipole magnetic field with strength $B_0 = 10^{12}$ G on the surface of the neutron star. Since the model fits are not sensitive to r_{in} , we are not able to constrain B_0 . Our results are not sensitive to the value of the outer disk radius r_{out} either, since the viscous timescale along the disk is much longer than the enhancement episodes of AXPs. In our calculations, we take $r_{\text{out}} = 10^{13}$ cm.

Irradiation parameter C represents the efficiency of X-ray irradiation flux $F_{\text{irr}} = (CMc^2)/(4\pi r^2)$ (Shakura & Sunyaev 1973), where \dot{M} is the mass accretion rate onto the neutron star. Infrared and optical data of the persistent AXPs can be accounted for by an active disk model with C in the range 10^{-4} – 10^{-3} (Ertan & Çalışkan 2006), similar to those estimated for low-mass X-ray binaries (LMXBs). Total X-ray luminosity is related to the mass accretion rate through $L = GMM/r$. We take $f = \dot{M}/\dot{M}_{\text{in}} = 1$, where \dot{M}_{in} is the mass-flow rate arriving at the innermost radius of the disk. Actually, f could be less than unity, that is, a fraction of \dot{M}_{in} can escape the system or may not return back to the disk. Employing lower f values in the calculations does not change our qualitative results but requires a modification of some other disk parameters. This will be discussed in Section 4. For comparison of the model with observations, we take the X-ray luminosities in the observational bands to represent the total X-ray luminosity of the source.

Different viscosity states prevail in the hot ($T > T_{\text{crit}}$) and cold ($T < T_{\text{crit}}$) regions of the disk. For the kinematic viscosity, we use the α -prescription (Shakura & Sunyaev 1973) with $\alpha = \alpha_{\text{cold}}$ and $\alpha = \alpha_{\text{hot}}$ in the cold and hot viscosity states, respectively. For a review of the DIMs, see, e.g., Lasota (2001). The disk evolution model we use here is the same as DIMs of LMXBs and dwarf novae (DNs). The difference is the value of the critical temperature, T_{crit} . In LMXB and DN disks, the thermal-viscous instability operates around the ionization temperature of hydrogen ($T_{\text{crit}} \sim 10^4$ K). In the case of AXPs, both the temperature profile and the chemical composition of the disk are different from the hydrogen disks of LMXB and DN. In AXP disks, metallicity is likely to be much higher than in an LMXB disk. We should also note that the hottest, innermost parts of the LMXB disks do not exist in AXP disks due to stronger dipole fields of AXPs that cut the disk at a relatively larger radius ($\sim 10^9$ cm).

The critical temperatures depend sensitively on the details of the ionization properties of the disk matter. Independent of these details, if the disk undergoes a global disk instability at a particular temperature, the resultant evolution of the disk produces a light curve that can be easily distinguished from the pure viscous decay curve (not affected by instabilities). Furthermore, fallback disks around AXPs are likely to have similar chemical compositions and similar critical temperatures.

In our model, there are five main disk parameters, namely, T_{crit} , α_{cold} , α_{hot} , p , and C , which govern the evolution of the accretion disk for a given initial mass distribution. Among these, T_{crit} and C are degenerate parameters. There is a constraint on the range of C obtained in our earlier work on the persistent AXPs (Ertan & Çalışkan 2006). These basic disk parameters are very likely to have similar values for fallback disks of different AXPs. In Section 2.2, we investigate the effects of model parameters on the evolution of the disk to clarify the subsequent discussion on the light curves of persistent and transient sources.

2.2. Parameter Study

Observations of X-ray outburst (enhancement) light curves of different AXPs with different energetics and timescales provide an opportunity for a detailed test of the fallback disk model and also for constraining the model parameters. In this section, we investigate the effect of important disk parameters on the X-ray outburst light curves of model sources.

2.2.1. Different Burst Energies

Soft gamma-ray bursts of AXPs are likely to have magnetic origin and to occur close to the neutron star. Assuming an isotropic emission, a small fraction $\delta E/E_{\text{tot}} \sim H_{\text{in}}/r_{\text{in}}$ of the total burst energy, E_{tot} , is absorbed by the disk, where δE is the part of the burst energy illuminating the disk and H_{in} is the half-thickness of the disk at $r = r_{\text{in}}$. H/r is roughly constant along the disk and is about 10^{-3} in the accretion regime of AXPs. When the inner disk is pushed back and heated by δE , part of the inner disk matter could escape the system, while the remaining part piles up, forming a surface density gradient at the inner disk (see Ertan et al. 2006 for details). In our model, the Gaussian surface density distribution represents the inner pileup and the power-law surface density distribution stands for the outer extended disk that is expected to remain unaffected by the soft gamma-ray burst. The position r_0 and the total mass δM of the pileup, for a given δE , depend on the inner disk radius r_{in} and the mass distribution of the inner disk just before the burst event. In steady state, the surface density profile of the inner disk–magnetosphere boundary is not well known. Assuming that the inner disk conditions are similar for fallback disks of AXPs, it is expected that a higher burst energy pushes the inner disk to a larger radius and creates a greater density gradient at the inner disk.

In the quiescent state, the mass-flow rate, \dot{M} , decays very slowly and therefore can be taken as constant in the models. In this steady state, $\dot{M} \propto \Sigma \nu$, where $\nu = \alpha c_s H$ is a function of temperature and radius and depends also on the ionization properties of the disk matter. The pressure scale height of the disk $H \simeq c_s/\Omega_K$, and then $\nu \propto T r^{3/2} \propto r^{3/4}$ (see, e.g., Frank et al. 2002), where T is the mid-plane temperature of the disk. The irradiation temperature $T_{\text{irr}} \propto r^{-1/2}$ modifies the effective temperatures and the stability criteria of the disk without significantly affecting the mid-plane temperatures in the accretion regime of AXPs and SGRs (e.g., Dubus et al. 1999). Then, in the quiescent state, the surface density of the disk $\Sigma \propto r^{-p}$ with $p = 3/4$. The main role of the irradiation is to slow down the decay of the X-ray luminosity, preventing the rapid propagation of the cooling front inward. This will be investigated in detail in Section 2.2.3.

We first illustrate X-ray enhancement light curves of a model source with different δM values representing the evolution of the same source with different burst energies. In the first exercise, we compare the model curves without invoking the instability (pure viscous evolution) with $\alpha = 0.1$, $r_{\text{in}} = 10^9$ cm, and $r_{\text{out}} = 10^{13}$ cm. Three different illustrative light curves presented in Figure 1 are obtained with different δM values that give peak luminosities of 1×10^{36} , 3×10^{36} , and 1×10^{37} erg s^{-1} . The quiescent L_X of all these sources are close to 10^{35} erg s^{-1} , a typical luminosity of a persistent AXP. It is seen that the X-ray luminosities follow almost the same decay curve after roughly a few months and eventually reach their quiescent level. For the first several weeks of the outburst both the fluences and the functional forms of the decay curves are

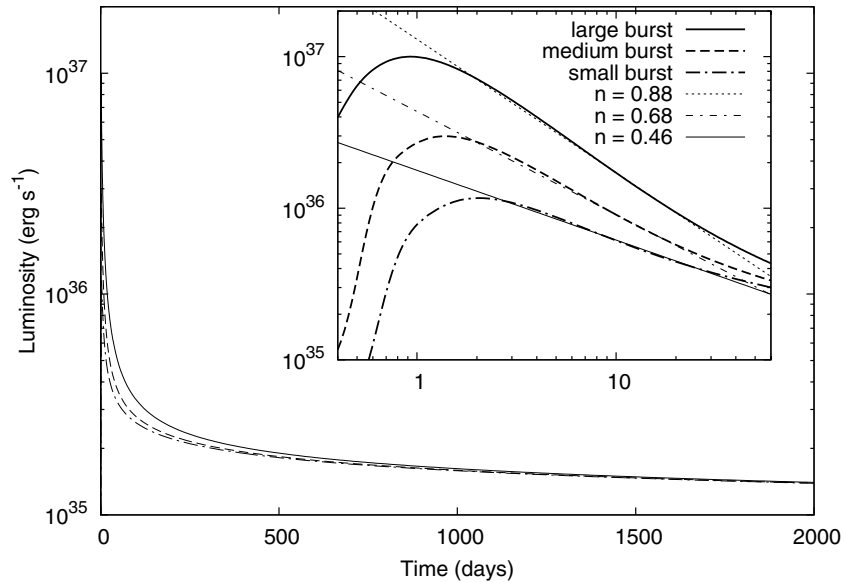


Figure 1. Model light curves produced by pure viscous evolution of disks for three different δE values. The short-term light curve, in the inset, shows peak luminosities of 10^{37} erg s^{-1} , 3×10^{36} erg s^{-1} , and 10^{36} erg s^{-1} , which all decay to the same quiescent luminosity in the long term. The δM values are 4.9×10^{22} g, 2.1×10^{21} g, and 8.9×10^{20} g, and the estimated δE values are 9.2×10^{39} erg, 3.8×10^{39} erg, and 1.7×10^{39} erg, respectively. The model light curves can be fitted with power laws in the early decay phase (roughly a few weeks). The values of power indices (n) are given in the inset.

very different from each other. For this initial decay phase, the model curves can be fit by a power law $L = L_{\text{peak}}(t/t_{\text{peak}})^{-n}$ with power-law indices of 0.88, 0.68, and 0.46. The minimum burst energy imparted to the disk can be estimated from δM using $\delta E \simeq GM\delta M(r_{\text{in}}^{-1} - r_0^{-1}) \simeq GM\delta M/r_{\text{in}}$. For these illustrative models, $\delta M = 4.9 \times 10^{22}$, 2.1×10^{22} , and 8.9×10^{21} g, and the estimated δE values are 9.2×10^{39} , 3.8×10^{39} , and 1.7×10^{39} erg, respectively. Note that actually a higher δE accumulates a greater δM at a larger r_0 . Since the chosen r_0 does not significantly affect the light curve, for simplicity, we take r_0 constant (5×10^9 cm) for all these illustrative simulations.

We repeat the same calculations for a model source with a quiescent luminosity around 10^{33} erg s^{-1} , typical for transient AXPs. In Figure 2, we present three different light curves produced by pure viscous evolution of the disk for three different δM values, without changing the other parameters. In this case, estimated δE values are 4.5×10^{38} erg, 2.3×10^{38} erg, and 1.2×10^{38} erg, respectively. For these sources, the first ~ 100 days of the decay curves can be fitted by power laws with indices 0.91, 0.73, and 0.59. In Figure 2, like the model sources given in Figure 1, the sources with higher δM show higher peak luminosities and sharper decay curves in this early phase of evolution.

In these examples, the model light curves are produced by pure viscous evolution of the disk without any instability. Comparing Figures 1 and 2, we might conclude that the sources with similar L_X in quiescence could show decay curves with rather different power-law indices, while it is also possible that sources with different quiescent luminosities could give similar decay curves in the early decay phase of the outburst. In Section 2.2.2, we show that this early phase of the X-ray light curves can indeed be produced by pure viscous evolution of the disk for both transient and persistent sources. This pure viscous evolution model gives similar long-term curves for all model sources (Figures 1 and 2), which would be the case if there were no critical temperature leading to viscous instability in the disk. In the following sections, we show how the presence of a critical temperature leads to systematic differences in the

functional form of the decay curves depending on the X-ray luminosities in quiescence.

2.2.2. Quiescent X-Ray Luminosity and Critical Temperature

The main characteristics of X-ray outbursts of soft X-ray transients (SXTs) and DNs can be successfully accounted for by DIMs (see, e.g., Lasota 2001 for a review). In these systems, the viscous instability manifests itself at temperatures around 10^4 K, which corresponds to the ionization temperature of hydrogen. In the DIMs, disk regions with temperatures higher and colder than this critical temperature are in hot and cold viscosity states, respectively. Different α parameters are employed in the cold and hot states ($\alpha_{\text{hot}} \sim 0.1$ and $\alpha_{\text{cold}} \sim 0.01-0.05$; see Section 2.2.4) to obtain reasonable model fits to the X-ray outburst light curves of SXTs and DNs. We note that these viscosities are turbulent in both hot and cold states.

We now investigate the effect of viscous instability with different critical temperatures on the model X-ray light curves of two illustrative sources with quiescent X-ray luminosities of 10^{33} and 10^{35} erg s^{-1} as representatives of transient and persistent AXPs. For both model sources, we take $C = 1 \times 10^{-4}$. The results are seen in Figure 3. Panel (a) shows the luminosity evolution of a persistent source, for three different T_{crit} values, as well as the pure viscous decay (no viscous instability). Similarly, panel (b) shows the evolution of a transient source. For a given source, the model curves with higher T_{crit} values diverge from the pure viscous decay curve earlier. Comparing Figures 3(a) and (b), we see that for a particular T_{crit} , the light curve of the persistent sources (high quiescent luminosity) deviates from the pure viscous decay curve much later than the transient sources (low quiescent luminosity). For instance, for $T_{\text{crit}} = 2000$ K, the light curve of the transient source deflects from the pure viscous decay curve at $t \sim 100$ days. For the persistent source with the same T_{crit} , the deviation starts at $t \sim 200$ days and the luminosity decreases much slower compared to the transient source. For $T_{\text{crit}} \sim 1500$ K, the light curve of the persistent source is indistinguishable from the pure viscous decay until $t \sim 400$ days, while for the transient source, the deviation starts as

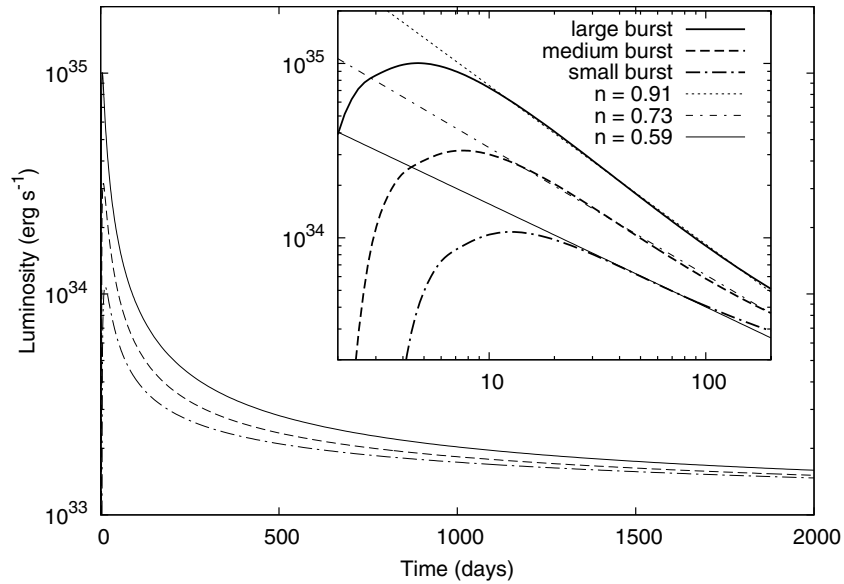


Figure 2. Short-term and long-term model light curves of a typical transient source for three different δE values. For these models, δM values are 2.4×10^{21} g, 1.2×10^{21} g, and 6.4×10^{20} g and estimated δE values are 4.5×10^{38} erg, 2.3×10^{38} erg, and 1.2×10^{38} erg, respectively. The decay phases of the light curves can be fitted with power laws for the first ~ 100 days (inset). The values of power indices (n) are given in the inset.

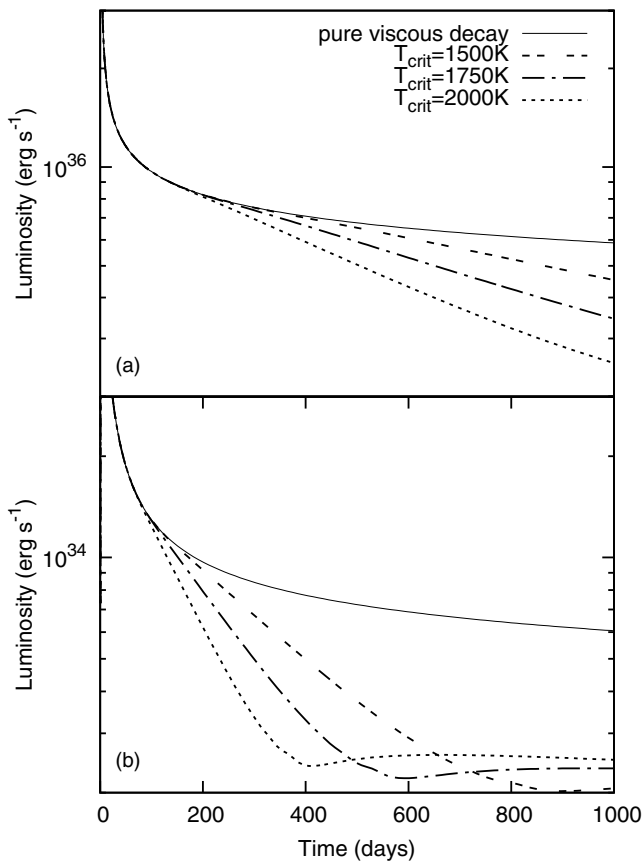


Figure 3. Model light curves for persistent (a) and transient (b) sources, for $T_{\text{crit}} = 1500$ K, 1750 K, and 2000 K. Solid curves illustrate the pure viscous decay with the same initial conditions for comparison. For a given T_{crit} , comparing (a) and (b), the difference between the model curves of the transient and persistent sources is clearly seen.

early as $t \sim 200$ days (Figure 3). This characteristic difference in the light-curve morphologies of high- and low-luminosity AXPs in the decay phase is mainly due to the differences in the surface density and temperature profile of the disks in the quiescent

states. These properties could be estimated from the X-ray luminosities in quiescence, which scales with the accretion rate onto the neutron star.

2.2.3. X-Ray Irradiation

Another factor that plays an important role in the evolution of the disk and the X-ray luminosity is the X-ray irradiation of the disk. The irradiation flux can be written as $F_{\text{irr}} = CMc^2/4\pi r^2$, where irradiation efficiency C depends on the albedo of the disk faces and the irradiation geometry (Shakura & Sunyaev 1973). The critical temperature discussed in Section 2.2.2 and C are degenerate parameters. The results of our earlier work on the X-ray and IR data of AXPs constrain the value of C to the range 10^{-4} – 7×10^{-4} (Ertan & Çalışkan 2006), which remains in the range of the estimated irradiation efficiencies of SXTs (10^{-4} – 10^{-3} ; de Jong et al. 1996; Dubus et al. 1999; Tuchman et al. 1990).

The effective temperature of a steady disk at a radial position is determined by the dissipation rate given by $D = 9\nu\Sigma\Omega_K^2/8$, where Ω_K is local Kepler velocity, and by the X-ray irradiation flux F_{irr} . Including F_{irr} , the effective temperature can be written as $\sigma T_{\text{eff}}^4 \simeq D + F_{\text{irr}}$. Since $\nu\Sigma \propto \dot{M}$, both F_{irr} and D have the same \dot{M} (and thus L_X) dependence. The irradiation flux and the dissipation rate decrease with radial distance as r^{-2} and r^{-3} , respectively. Equating F_{irr} to D , we find $r \sim 2 \times 10^9$ cm, which does not depend on \dot{M} . For smaller radii, D dominates F_{irr} , while F_{irr} is the dominant source of heating beyond this radius (see, e.g., Frank et al. 2002).

The radius r_h of the hot inner disk is determined by the strength of the X-ray irradiation ($T(r = r_h) = T_{\text{crit}}$). Increasing (decreasing) F_{irr} increases (decreases) the effective temperatures at all radii, and r_h is situated farther out (in). This implies that the sources with higher X-ray luminosity have greater r_h . This is actually the main reason that leads to different X-ray light-curve morphologies in the enhancement phases of transient and persistent sources. The rate of mass accretion that powers L_X is determined by the surface density profile of the disk. The sources with higher surface densities have higher accretion rates, higher

X-ray irradiation fluxes, and thus greater r_h . To illustrate, for $T_{\text{crit}} = 1500$ K and $C = 1.5 \times 10^{-4}$, we find $r_h = 1.4 \times 10^{11}$ cm for $L_X = 10^{35}$ erg s $^{-1}$ and $r_h = 1.4 \times 10^{10}$ cm for $L_X = 10^{33}$ erg s $^{-1}$.

At the beginning of the X-ray enhancement phase, the innermost disk that was emptied by the burst is refilled rapidly due to high density gradients, leading to a sharp rise in X-ray luminosity. The mass-flow rate in the inner disk, the accretion rate onto the neutron star, and thereby the X-ray luminosity, L_X , and r_h reach their maximum values. Subsequently, r_h decreases gradually at a rate governed by the decreasing X-ray flux.

In the quiescent phase, the mass-flow rate at the inner hot disk depends on the conditions at the cold outer disk. The hot disk easily transfers all the mass flowing from the outer cold disk toward r_{in} . During an enhancement, the mass-flow rate is determined mainly by the viscous processes at the hot inner disk. Just before the onset of the X-ray outburst, the total amount of mass that remains within r_h , the position of r_h , and the rate at which it moves inward all affect, and also depend on, the evolution of L_X .

Initially, the light curve mimics that of a pure viscous decay, since the information from r_h moving inward reaches the inner disk after a viscous timescale across the hot disk. With decreasing r_h , the total hot mass contributing to the accretion with high viscosity also decreases. After the conditions at r_h start to modify \dot{M}_{in} , L_X decreases more rapidly and diverges from the pure viscous decay curve.

In Figure 4, we give the model curves with different C values, keeping $T_{\text{crit}} = 1750$ K for all the simulations. Comparing with Figure 3, it is seen that the light curves for different C values are similar to those obtained with different T_{crit} values, keeping C constant. It is also seen that the viscous instabilities triggered at the same T_{crit} and with the same C produce very different light curves for transient and persistent sources.

2.2.4. Viscosity Parameter

For both transient and persistent AXPs, the rise, turnover, and early decay phase (several weeks to months) of the X-ray light curve are produced by the evolution of the hot inner disk matter and the resultant accretion onto the neutron star. In all our calculations, we take $\alpha_{\text{hot}} = 0.1$ as in our earlier works. For all the sources, this initial phase of the light curve is indistinguishable from that produced by a pure viscous evolution of the disk, that is, the evolution of a disk remaining in the same viscosity state at all radii. By illustrative model light curves (Figures 3–5), we have shown that the deviation from this pure viscous decay phase starts much earlier in transient AXPs that have relatively low luminosities in the quiescent phase. After the instability starts to affect the accretion rate, the value of α_{cold} has an important role in the evolution of the X-ray luminosity L_X . From the DIMS of SXTs and DNs, α_{cold} is estimated to be ~ 0.01 – 0.05 (Lasota 2001). From model fits to the X-ray enhancement light curve of XTE J1810–197, Ertan & Erkut (2008) found that $\alpha_{\text{cold}} \sim 0.03$ with $T_{\text{crit}} \sim 1500$ K produce reasonable model curves. In the present work, we also refine the model parameters of Ertan & Erkut (2008) through a comparative study with the X-ray enhancement light curves of other transient AXPs, including the new data points of XTE J1810–197 (Section 3).

Keeping all the other parameters constant, we see that small variations in α_{cold} could lead to significant changes in the light curve at the end of the decay phase. To illustrate this effect,

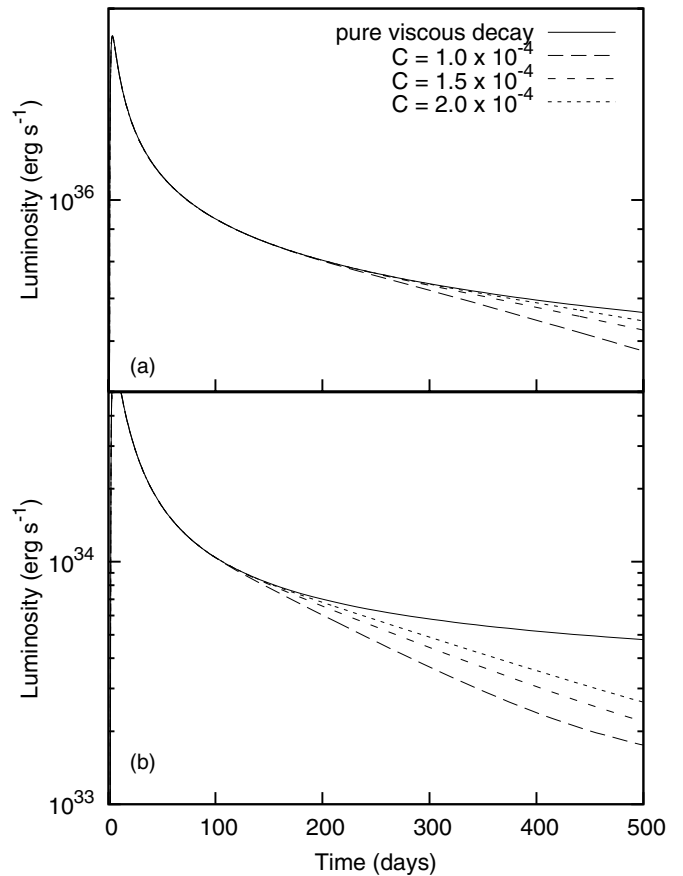


Figure 4. (a) Model light curves of a persistent source for different C values; (b) light curves for a transient source, for the same parameter values. The model curves representing pure viscous decay are given with solid lines and $T_{\text{crit}} = 1750$ K for the other models. It is seen that the evolution of persistent sources diverges from the pure viscous decay curve much later than transients.

we present model curves with different α_{cold} values in Figure 5. The depths of the minima at the end of the model light curves of the model sources depend mainly on the values of α_{cold} . It is seen in Figure 5 that the model light curves settle down to the quiescent level following quite different morphologies even for small changes in α_{cold} .

The physical reason producing the minima in the model curves can be summarized as follows: after the formation of the pileup at the inner disk, the accretion rate abruptly increases in the hot disk region ($r < r_h$) due to newly formed density gradients. The resultant increase in L_X pushes r_h to larger radii, causing part of the previously cold disk region to enter the hot viscosity state. Due to the density gradients and more efficient kinematic viscosity in the hot state, the inner disk matter is depleted at a rate much higher than the mass-flow rate provided by the outer disk. As a result, surface density profile $\Sigma(r)$ of the inner disk decreases below the extrapolation of $\Sigma(r)$ of the cold outer disk. Meanwhile, L_X decreases due to the decreasing Σ of the inner disk and the propagation of r_h inward with decreasing L_X .

The rate of refilling of the innermost disk regions sensitively depends on the value of α_{cold} . It is seen in Figure 5(b) that the minimum in the model light curves becomes more pronounced for smaller α_{cold} values. This is because the surface density gradients are smoothed out more rapidly with higher kinematic viscosity. Observed X-ray enhancement light curves provide an opportunity to constrain the value of α_{cold} . Nevertheless, the

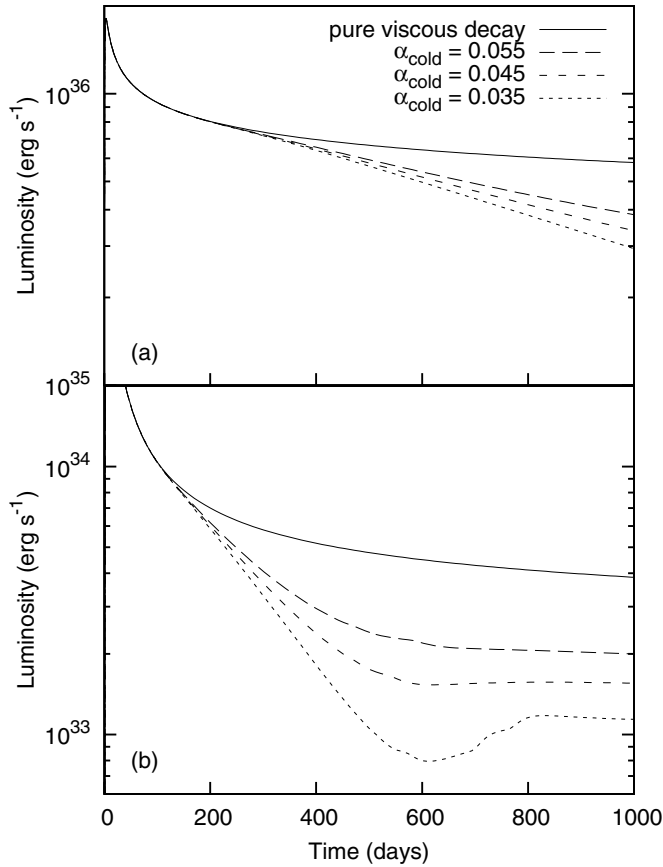


Figure 5. (a) Light curve of a persistent source for different α_{cold} values; (b) light curves for a transient source, for the same parameter values. The pure viscous decay curves are also presented (solid lines) for comparison. For the other models, we take $T_{\text{crit}} = 1750$ K and $C = 1 \times 10^{-4}$.

limitation for testing the models can also be clearly seen in Figure 5(b). The accretion luminosity of the transient AXPs might decrease even below the intrinsic cooling luminosity of the neutron star depending on the age of the source.

2.2.5. Outer Disk Radius

The outer disk radius, r_{out} , defines the extent of the active accretion disk and depends on the minimum disk temperature at which the disk becomes inactive. X-ray luminosity and rotational and statistical properties of AXPs can be explained by the long-term evolution of neutron stars evolving with fallback disks that become inactive at low temperatures around ~ 100 – 200 K (Ertan et al. 2009). In this model, r_{out} gradually decreases in time with slowly decreasing quiescent X-ray luminosity of the source.

The evolution of r_{out} has an important effect on the long-term (10^3 – 10^5 yr) evolution of AXPs. Nevertheless, the position of r_{out} does not affect the X-ray enhancement light curves of AXPs, which last from months to several years. The outer radii of the fallback disks of known AXPs are estimated to be greater than about a few $\times 10^{12}$ cm (Ertan et al. 2007). The viscous timescale across the disk is longer than the duration of the enhancement phase. In our calculations, we set $r_{\text{out}} = 10^{13}$ cm. We note that the radius r_{h} of the hot disk, which is the border between low- and high-viscosity regions of the disk, should not be confused with r_{out} .

3. APPLICATION OF THE MODEL TO THE X-RAY ENHANCEMENT LIGHT CURVES OF TRANSIENT AXPs

Our model parameters and their effects on the evolution of the sources are described in detail in Section 2. Now, we test this model, performing model fits to the X-ray outburst light curves of the sources XTE J1810–197, SGR 1627–41, CXOU J164710.2–455216, and SGR 0501+4516 (Figures 6–9). The model parameters are presented in Table 1. All these sources were detected in the decay phases of their X-ray outbursts. The rise and turnover phases of the outburst were missed.

The X-ray flux of XTE J1810–197 in quiescence (during 1993–1999) was 5.5×10^{-13} erg cm $^{-2}$ s $^{-1}$ (Gotthelf et al. 2004) and increased to about 5.5×10^{-11} erg cm $^{-2}$ s $^{-1}$ during the outburst (Ibrahim et al. 2004). Most recent distance and corresponding peak luminosity estimates for this source are $d = 5$ kpc, $L_X = 1.3 \times 10^{36}$ erg s $^{-1}$ (Ibrahim et al. 2004), $d = 3.3$ kpc, $L_X = 5.8 \times 10^{35}$ erg s $^{-1}$ (Lazaridis et al. 2008), and $d = 3.5$ kpc, $L_X = 6.6 \times 10^{35}$ erg s $^{-1}$ (Bernardini et al. 2009). In our calculations, we take $d = 3.5$ kpc. For the model fits, we use 2–10 keV X-Ray Timing Explorer (XTE) data (Ibrahim et al. 2004) and 0.6–10 keV *XMM* data (Bernardini et al. 2009). The *XMM* data were converted to 0.1–10 keV unabsorbed flux with *WebPIMMS*, using the 3BB model described in their paper. The XTE data, given in counts s $^{-1}$ PCU $^{-1}$, were converted to unabsorbed flux using a conversion factor. The factor was chosen so as to align the first *XMM* data with the corresponding XTE data (in 2003 September). Our model curve is given in Figure 6. For all the sources, together with the best model fits, we also plot the pure viscous decay curves for comparison.

The transient SGR 1627–41 underwent an X-ray outburst in 1998, and its decay curve is also similar to those of other transient sources (Mereghetti et al. 2006). The peak luminosity of SGR 1627–41 was 9.5×10^{34} d $_{11}^2$ erg s $^{-1}$ during the outburst, and the distance was measured as 11.0 ± 0.3 kpc (Corbel et al. 1999). The source subsequently decayed to quiescence with $L_X \sim 3.9 \times 10^{33}$ d $_{11}^2$ erg s $^{-1}$ (Kouveliotou et al. 2003). In 2008 May, a new X-ray outburst was observed in SGR 1627–41 (Palmer et al. 2008). The absorbed 2–10 keV flux was $\sim 1.3 \times 10^{-12}$ erg cm $^{-2}$ s $^{-1}$, corresponding to a luminosity of $L_X \sim 3 \times 10^{34}$ d $_{11}^2$ erg s $^{-1}$ (Esposito et al. 2009). There is an uncertainty in estimating the unabsorbed flux of this source due to high interstellar absorption with $N_{\text{H}} \sim 10^{23}$ cm $^{-2}$ (Mereghetti et al. 2009). We take $d = 11$ kpc to estimate the luminosity. Our model curve is seen in Figure 7.

A soft gamma-ray burst from CXOU J164710.2–455216 was detected with *Swift* BAT on 2006 September 21 (Krimm et al. 2006). It was observed for ~ 20 ms with total energy $\sim 3 \times 10^{37}$ erg (15–150 keV, for $d = 5$ kpc; Munro et al. 2007). The observed maximum X-ray flux data point was reported 1.6 days after the burst. The X-ray flux data of AXP CXOU J164710.2–455216 cover about 150 days on the decay phase of its outburst in 2006 September (Israel et al. 2007; Woods et al. 2011). The X-ray luminosity of the source increased from $\sim 1 \times 10^{33}$ d $_5^2$ erg s $^{-1}$ to more than 1×10^{35} d $_5^2$ erg s $^{-1}$ during the outburst (Munro et al. 2007). The distance of CXOU J164710.2–455216, located in a star cluster, was estimated as $2 \text{ kpc} < d \leq 5.5 \text{ kpc}$ (Clark et al. 2005). We convert the flux data to luminosity using $d = 5$ kpc. The data seen in Figure 8 seem to be taken in the early decay phase of this source and therefore do not constrain T_{crit} yet.

Another transient source that was discovered in an outburst is SGR 0501+4516 (Barthelmy et al. 2008). Subsequently, the source was observed with *XMM-Newton*, *Swift*, and *Suzaku* in

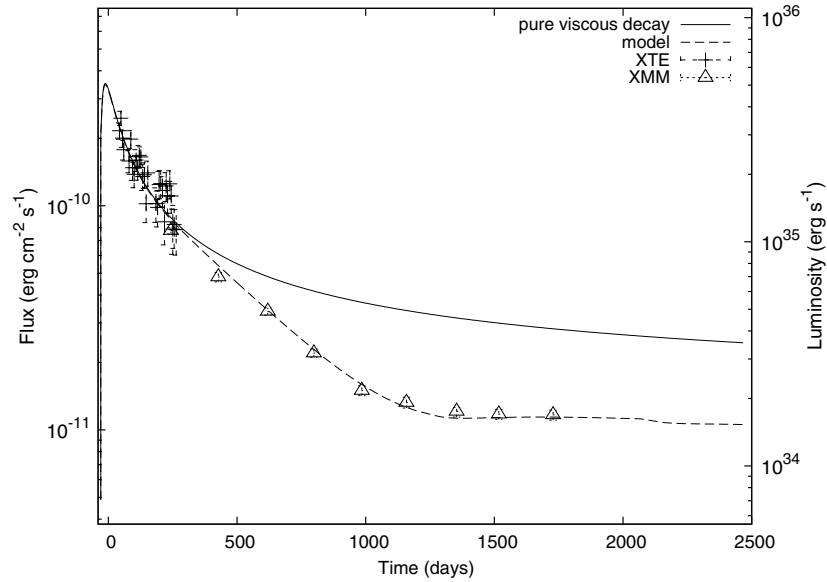


Figure 6. 0.1–10 keV unabsorbed X-ray flux and luminosity data of XTE J1810–197. The absorbed 0.6–10 keV *XMM* data (Bernardini et al. 2009) were converted to unabsorbed 0.1–10 keV flux using the 3BB model described in their paper. The XTE data were given in counts s^{-1} cpu^{-1} with a conversion factor for 2–10 keV absorbed flux (Ibrahim et al. 2004), with no spectral fits. The XTE data were rescaled by a factor of 2.3 to match the first *XMM* data, taken in 2003 September (see the text for details). The luminosity is calculated assuming $d = 3.5$ kpc. For this model, $\delta M \sim 1 \times 10^{23}$ g and the estimated $\delta E \sim 1 \times 10^{40}$ erg.

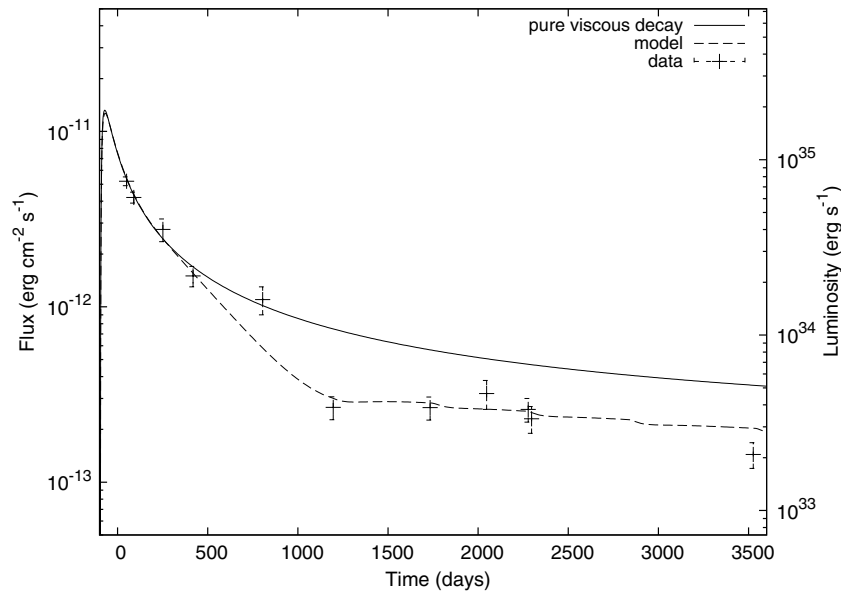


Figure 7. Unabsorbed 2–10 keV flux and luminosity data of SGR 1627–41 (Mereghetti et al. 2006). The parameters of the model curve, given by the dashed line, are listed in Table 1. The solid curve represents pure viscous decay with the same initial conditions. These model curves are obtained with $\delta M \sim 4 \times 10^{22}$ g, which gives $\delta E \sim 4 \times 10^{39}$ erg with the chosen r_{in} (see the text for details). The luminosity is calculated assuming $d = 11$ kpc.

the decay phase, starting from a maximum absorbed 1–10 keV flux of 4.1×10^{-11} $erg\ cm^{-2}\ s^{-1}$ (Rea et al. 2009; Figure 9). The distance of SGR 0501+4516 is not very well determined, with estimates $d = 1.5$ kpc (Aptekar et al. 2009), $d = 4$ kpc (Nakagawa et al. 2011), $d = 5$ kpc (Rea et al. 2009), and $d = 10$ kpc (Enoto et al. 2009; Kumar et al. 2010). The pre-outburst quiescent (0.1–2.4 keV) flux of this source was reported as $\sim 4.1 \times 10^{-12}$ $erg\ cm^{-2}\ s^{-1}$ (Rea et al. 2009), which corresponds to a 1–10 keV flux of 1.3×10^{-12} $erg\ cm^{-2}\ s^{-1}$. Assuming a distance of 5 kpc, the maximum and quiescent luminosities are 1.2×10^{35} $erg\ s^{-1}$ and 4×10^{33} $erg\ s^{-1}$, respectively. We take $d = 5$ kpc in our calculations.

The transient AXP 1E 1547.0–5408 at the end of the ~ 100 days of decay showed re-brightening (Camilo et al. 2008), possibly due to another soft gamma-ray burst, which we could

not address in the model. Long-term behavior of this source can be studied by future observations. The source showed SGR-like flaring activity in 2009 January, observed by *INTEGRAL* and *Swift* (Savchenko et al. 2010).

The X-ray flux data of the candidate transient AXP AX J1845–0258 cover a period of longer than 10 years. Tam et al. (2006) argue that the recent flux data of AX J1845–0258 may be from another unrelated source within the error circles. Because of this ambiguity, we did not include this source in the present work.

The decay timescales of XTE J1810–197 and SGR 1627–41 are a few years (see Figures 6 and 7). The transient sources CXOU J164710.2–455216 and SGR 0501+4516 seem to have been observed while still in their early decay phases ($t \sim 150$ days). In Figures 8 and 9, we also present the estimated

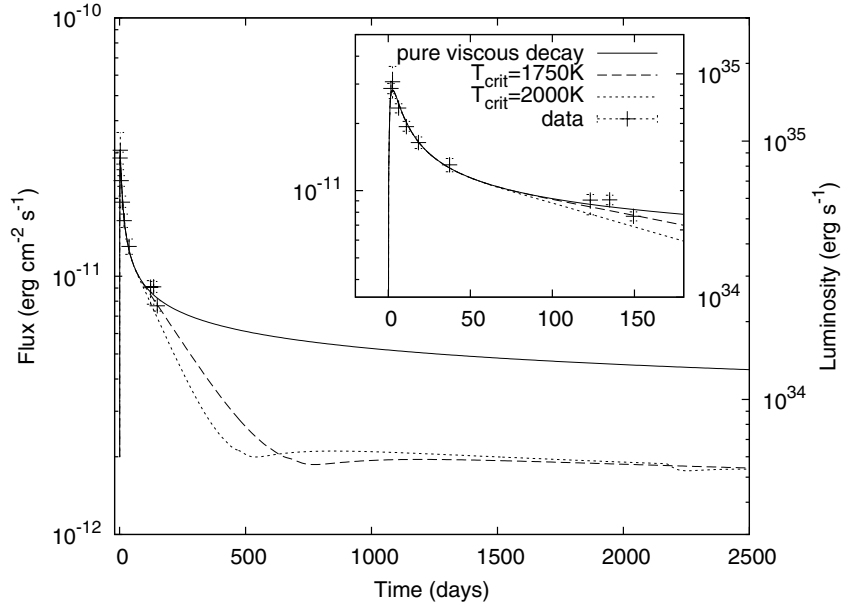


Figure 8. Unabsorbed 2–10 keV flux data of CXOU J164710.2–455216 (Israel et al. 2007; Woods et al. 2011). The long-term model light curves are obtained with $T_{\text{crit}} = 1750$ K and $T_{\text{crit}} = 2000$ K. For these models, $\delta M \sim 2 \times 10^{21}$ g and the estimated $\delta E \sim 2 \times 10^{38}$ erg. The luminosity is calculated assuming $d = 5$ kpc.

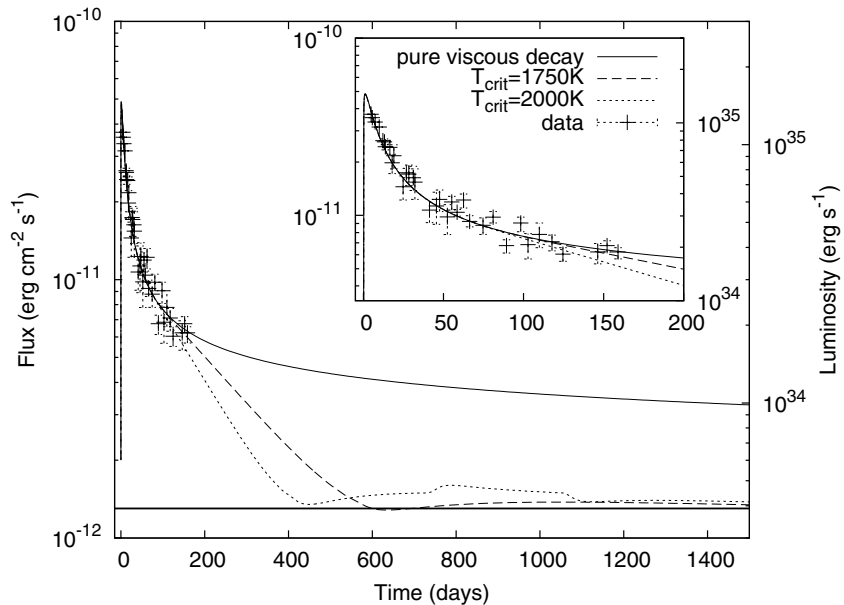


Figure 9. Absorbed 1–10 keV flux and luminosity data of SGR 0501+4516 (Rea et al. 2009). The model light curves are obtained with $T_{\text{crit}} = 1750$ K and $T_{\text{crit}} = 2000$ K. The horizontal line shows the estimated quiescent flux of the source (1.3×10^{-12} erg cm $^{-2}$ s $^{-1}$), obtained from *ROSAT* observations in 1992, extrapolated to the 1–10 keV band assuming a blackbody emission (Rea et al. 2009). The luminosity is calculated assuming $d = 5$ kpc. These model curves are obtained with $\delta M \sim 3 \times 10^{21}$ g. We estimate $\delta E \sim 2 \times 10^{38}$ erg. It is seen that the source is about to diverge from the pure viscous decay curve (solid curve).

evolution of these sources in the future for different T_{crit} values. We note that the decay characteristics of the model light curves depend on the quiescent level of X-ray luminosity or accretion rate. Any corrections in distance measurements may require a revision of some model parameters.

4. RESULTS AND DISCUSSION

Our model calculations show that the idea proposed by Ertan & Erkut (2008) to explain the X-ray enhancement light curve of XTE J1810–197 can be extended to other transient AXPs as well. This idea could be summarized as follows: there is a critical temperature, $T_{\text{crit}} \sim 2000$ K, that prevails in the

fallback disks of all AXPs. In the X-ray enhancement phase, the viscous instability created at this temperature governs the X-ray luminosity starting from a certain time of the decay phase, depending mainly on the disk properties in quiescence. The properties of the extended disk, in particular the surface density profile, can be estimated from the X-ray luminosity in quiescence, which is different in low-luminosity transient and high-luminosity persistent AXPs. Because of these differences in the disk properties, the effect of the instability on the decay curve is more pronounced and starts earlier in the transient AXPs than in persistent AXPs (see Section 2.2 and Figures 3–5).

A self-consistent explanation of the observed X-ray light curves requires that the basic model parameters obtained for

Table 1
The Parameters for the Model Curves Presented in Figures 6–9

Parameter	XTE J1810–197	SGR 1627–41	CXO J164710.2–455216	SGR 0501+4516
r_{in} (cm)	2×10^9	2×10^9	1.8×10^9	3×10^9
r_0 (cm)	7×10^9	2.3×10^{10}	5×10^9	6×10^9
Δr (cm)	9×10^9	6×10^8	6×10^8	1.4×10^9
Σ_{max} (g cm^{-2})	20	60	13	10
Σ_0 (g cm^{-2})	10	1	7.6	5
α_{hot}	0.1	0.1	0.1	0.1
α_{cold}	0.045	0.045	0.045	0.045
T_{crit} (K)	1750	1750	1750	1750
C	1×10^{-4}	1.6×10^{-4}	1×10^{-4}	1×10^{-4}
p	0.75	0.75	0.75	0.75

Notes. Note that the parameters α_{hot} , α_{cold} , p , and T_{crit} are expected to be similar for all AXPs and SGRs. Irradiation efficiency, C , which could change with accretion rate, is also likely to be similar for the sources in the same accretion regimes. In quiescence, Σ_0 scales with accretion rate. The parameters Δr , r_0 , and Σ_{max} could vary from source to source, depending on the burst energy and geometry. The values of inner disk radius r_{in} are close to the Alfvén radii of the sources with $B_0 \simeq 10^{12}$ G. We set $r_{\text{out}} = 10^{13}$ cm and $f = \dot{M}/\dot{M}_{\text{in}} = 1$ for all our models.

the different enhancement light curves of AXPs should be similar within the uncertainties of the fallback disks. These basic parameters, which are described in detail in Section 2.2, are the viscosity parameters in the cold and hot state of the disk (α_{cold} , α_{hot}), the irradiation parameter (C), the critical temperature (T_{crit}), and the power index (p) of the initial surface density profile, $\Sigma \propto r^p$, of the extended disk. It is seen in Table 1 that these parameters of our model for different AXPs are either the same or very close to each other. With these parameters, the model X-ray light curves for four different transient AXPs are in good agreement with observations (Figures 6–9).

X-ray enhancement of persistent AXPs can also be fit well by the pure viscous evolution model (Ertan & Alpar 2003; Ertan et al. 2006). This is consistent with our results, since the critical temperatures found here do not significantly affect the enhancement light curves of persistent AXPs (Section 2).

The model that we use in the present work was first proposed by Ertan & Alpar (2003) for SGR 1900+14. The only difference in our work is that we introduce a critical temperature (T_{crit}). It is the presence of this T_{crit} that leads to viscous instability during the enhancement phase. In the model, this instability does not produce an X-ray outburst but changes the evolution of the disk mass-flow rate and thereby the X-ray luminosity in the decay phase of the X-ray enhancement. In the disk, at temperatures below and above T_{crit} we use different alpha parameters (α_{hot} and α_{cold}) to represent different viscosity states like in the models of SXTs. Over the decay phase, in the disk, the radius with $T = T_{\text{crit}}$ (cooling front) propagates inward as we explained in Sections 2.2.3 and 2.2.4. In this phase, the rapid motion of the cooling front with varying X-ray luminosity is a viscous instability since it changes the viscosities along the radii it propagates. On the other hand, in the model, the observed X-ray enhancement is produced by the mass density and temperature gradients at the inner disk.

The effect of this propagation of the cooling front on the X-ray light curve is remarkably different in low-luminosity transient and high-luminosity persistent systems like SGR 1900+14, and this was discussed in detail with illustrative model curves in the paper. All X-ray enhancement light curves of AXP/SGRs mimic the light curve produced by a pure viscous decay in the early phase of evolution, but later, they diverge from the pure viscous decay curve due to ongoing viscous instability in the disk (Figures 3–5). The same T_{crit} exists in all fallback disks;

nevertheless, the effect of the cooling-front propagation in the decay phase is more prominent and observed earlier from the systems that have lower luminosities in the quiescent state. In the present work, we also present the model curves produced by pure viscous decay just to show, by comparison, the effect of the instability on the luminosity evolution of the sources.

The fact that Ertan & Alpar (2003) can fit to the enhancement light curve of SGR1900+14 with a single alpha parameter ($\alpha_{\text{hot}} \sim 0.1$), without using a T_{crit} , indicates that the information from the cooling front could not communicate to the innermost disk during the observation period of this source. That is, when T_{crit} with values obtained in our work is inserted in Ertan & Alpar (2003), their model curve does not change. This shows the self-consistency of our results with the earlier work and could also be tested by the future observations of these sources. Since the critical temperature depends on the details of the chemical composition of fallback disks, which is not well known, it could only be estimated from the model fits. Considering that this critical temperature must be an intrinsic property of the fallback disks, its value must be the same in all AXP/SGR systems. In the present work, we also constrain this critical temperature, trying to find solutions that can fit the light curves of all these transient sources with a similar T_{crit} along with other similar sets of intrinsic disk parameters (Table 1).

In the quiescent state, the position of the cooling front remains almost constant and is determined by the current X-ray irradiation flux. In quiescence, back-and-forth motion of the cooling front in a narrow radial region of the disk could create variations in the local mass-flow rate (and could still be called viscous instability), but those are smoothed out on the way to the Alfvén radius and do not cause variations in the X-ray luminosity. Therefore, we expect to observe the effect of the viscous instability in the decay phase of the X-ray luminosity.

We note that, in the present work, we have also refined the model parameters obtained by Ertan & Erkut (2008) for XTE J1810–197 considering the newly reported last three data points of this source (Bernardini et al. 2009). Illustrative model curves given in Ertan & Erkut (2008) can produce the 2–10 keV absorbed data¹ for a particular α_{cold} . Nevertheless, these model curves are seen to remain above the new data points by a factor

¹ There is a misprint in the label of Figure 1 in Ertan & Erkut (2008). The data in their Figure 1 are absorbed flux.

of three. We notice that the interstellar absorption significantly affects the light curve of the source close to the quiescent level of the X-ray luminosity. Here, we have repeated the calculations using unabsorbed data including the new data points of the source (Bernardini et al. 2009). For also the other sources, except for SGR 0501+4516, we have used unabsorbed data (Ibrahim et al. 2004; Bernardini et al. 2009; Mereghetti et al. 2006; Israel et al. 2007; Woods et al. 2011; Rea et al. 2009). Since SGR 0501+4516 is in the early decay phase of the X-ray outburst (Figure 9), its absorbed data can be safely used to test our model. The model curves presented in Figures 6–9 are obtained with degenerate parameters $T_{\text{crit}} = 1750$ K and $C \simeq 1 \times 10^{-4}$. For the maximum possible value of C ($\sim 7 \times 10^{-4}$), indicated by our earlier work, reasonable light curves could be obtained by increasing T_{crit} by a factor of ~ 1.6 . This constrains T_{crit} to the ~ 1700 – 2800 K range. This is not a strong constraint, since this result was obtained with a particular $f = \dot{M}/\dot{M}_{\text{in}} = 1$ (see Section 2.1). Reasonable model curves can also be obtained with lower f values; nevertheless this requires modification of the model parameters. For instance, using $f = 0.1$, a model curve that fits well to X-ray enhancement data of XTE J1810–197 can be obtained with $\alpha_{\text{cold}} = 0.039$ and 1350 K $< T_{\text{crit}} < 2100$ K, corresponding to $1 \times 10^{-4} < C < 7 \times 10^{-4}$.

In Figures 6–9, we also give the estimated mass δM of the pileup for each of the sources. Our results sensitively depend on δM . Estimated amount of burst energy δE imparted to the inner disk depends on δM , r_{in} and r_0 . Relative positions of r_{in} and r_0 also affect the model light curves, while similar results could be obtained with different r_{in} values, adjusting r_0 and surface density without changing δM . There is an uncertainty in estimated δE because of the uncertainties in r_{in} and surface density profile of the innermost disk in quiescence.

In the case of SGR 0501+4516, the distance is rather unconstrained (see Section 3). This source seems to be in the early phase of evolution, at a time the information from the cooling front has not reached the innermost disk by the viscous processes yet. This is the phase over which the light curve mimics that of a pure viscous decay. That is, changing the initial surface density profile at all radii by a constant multiplicative factor, it is possible to obtain different model light curves that have the same functional forms that differ only in amplitudes. Since any change in distance will modify all data points with the same multiplicative factor, we can obtain a similar model fit without modifying the intrinsic disk parameters. Nevertheless, after the viscous instability deviates the light curve from that of pure viscous decay, any correction in distances could require a modification of the critical temperature parameter to obtain a similar model fit to data, or possibly the model could fail in producing the observed light curve.

We should also note the possibilities of different burst geometries. We assume that the soft gamma-ray burst energy is emitted isotropically. This might not be the case, at least for some of the bursts. For instance, only a certain angular segment of the disk could be illuminated by the burst energy. This leads to a rather different post-burst surface density profile than we assume here. Even in this case, the resultant enhancement light curves are likely to be similar to those produced by an isotropic burst, provided that the burst creates a sufficient surface density gradient. These possibilities put further uncertainties on the estimated burst energy. For instance, in some cases it is possible that we observe an X-ray enhancement without observing the triggering burst whose anisotropic emission pattern evaded us. Another possibility is that we could observe bursts that are not

followed by an enhancement in X-rays, if the solid angle of this particular burst does not cross the disk.

Independent of the details of burst geometries, subsequent X-ray outburst light curves of different AXPs provide a good test for the fallback disk model. For given quiescent and peak X-ray luminosities in an enhancement phase, there is a single decay curve estimated by the disk model. To put it in other words, all the observed enhancement light curves of AXPs should be reproduced by a single set of main disk parameters.

In comparison of the model curves with data, there are some uncertainties that we encounter at very low luminosities ($L_X \sim 10^{33}$ erg s $^{-1}$): (1) due to very low temperatures, a significant fraction of the X-ray luminosity of the source is expected to be emitted below the observed X-ray band that we take to represent the total luminosity of the source. (2) Absorption effects considerably increase for the soft radiation emitted at these low temperatures. (3) Depending on the age, the cooling luminosity of the source could have significant contribution to the total quiescent luminosity of the source. (4) It is possible that some small bursts could be emitted in the decay phases and affect the secular decay characteristics of the light curves. It is not possible to address these effects in the model. For instance, the data point that remains above the model light curve of SGR 1627–41 (Figure 7) might be due to such a small burst.

Within these uncertainties, our model curves are in agreement with the X-ray enhancement data of four transient AXPs (Figures 6–9). We have succeeded to obtain reasonable model curves with almost the same basic disk parameters, given in Table 1.

5. CONCLUSIONS

We have shown that the X-ray outburst (enhancement) light curves of AXPs and SGRs can be explained by the evolution of an irradiated disk after the inner disk is pushed back to larger radii by a soft gamma-ray burst. A viscous instability created at a critical temperature, T_{crit} , seems to be a common property of all AXP/SGR disks. For the extreme values of X-ray irradiation efficiency obtained from our earlier work (Ertan & Çalışkan 2006), we estimate that T_{crit} is in 1300–2800 K range.

Characteristic differences between the enhancement light curves of transient and persistent AXP/SGRs can naturally be accounted for by their different pre-burst (quiescent) conditions of the disks implied by the X-ray luminosity of the sources in quiescence. X-ray outburst light curve of a persistent AXP/SGR could not be distinguished from a light curve produced by a pure viscous (without any instability) evolution of the disk for a few years. For a transient source, the outburst light curve could diverge from the pure viscous evolution within months after the onset of the outburst (Figures 6–9). These results are consistent with our earlier work on the X-ray outburst light curves of persistent AXP/SGRs (see, e.g., Ertan et al. 2006) which were explained by pure viscous evolution of the disk.

Basic properties of the fallback disks are likely to be similar in the fallback disks of all AXP/SGRs. Through a large number of simulations, we have obtained a single set of these basic parameters (Table 1) that can produce reasonable model fits to the enhancement light curves of four transient AXP/SGRs (Figures 6–9).

The predictions of our model could be tested by future observations of AXPs and SGRs in the X-ray enhancement phases.

We acknowledge research support from TÜBİTAK (The Scientific and Technical Research Council of Turkey) through grant 110T243 and from the Sabancı University Astrophysics and Space Forum. This work has been supported by the Marie Curie EC FPG Marie Curie Transfer of Knowledge Project ASTRONS, MKTD-CT-2006-042722. We thank Ali Alpar, Hakan Erkut, and Yavuz Ekşi for useful discussions and comments on the manuscript. We thank the anonymous referee for his/her useful comments.

REFERENCES

- Alpar, M. A. 2001, *ApJ*, 554, 1245
- Alpar, M. A., Ertan, Ü., & Çalışkan, Ş. 2011, *ApJ*, 732, L4
- Aptekar, R. L., Cline, T. L., Frederiks, D. D., et al. 2009, *ApJ*, 698, L82
- Barthelmy, S. D., Baumgartner, W. H., Beardmore, A. P., et al. 2008, *ATel*, 1676
- Bernardini, F., Israel, G. L., Dall’Osso, S., et al. 2009, *A&A*, 498, 195
- Camilo, F., Reynolds, J., Johnson, S., Halpern, J. P., & Ransom, S. M. 2008, *ApJ*, 679, 681
- Chatterjee, P., Hernquist, L., & Narayan, R. 2000, *ApJ*, 534, 373
- Clark, J. S., Negueruela, I., Crowther, P. A., & Goodwin, S. P. 2005, *A&A*, 434, 949
- Corbel, S., Chapuis, C., Dame, T. M., & Duroichoux, P. 1999, *ApJ*, 526, L29
- de Jong, J. A., van Paradijs, J., & Augusteijn, T. 1996, *A&A*, 314, 484
- Dubus, G., Lasota, J.-P., Hameury, J.-M., & Charles, P. 1999, *MNRAS*, 303, 139
- Duncan, R. A., & Thompson, C. 1992, *ApJ*, 392, 9
- Ekşi, K. Y., & Alpar, M. A. 2003, *ApJ*, 599, 450
- Enoto, T., Nakagawa, Y. E., Rea, N., et al. 2009, *ApJ*, 693, L122
- Ertan, Ü., & Alpar, M. A. 2003, *ApJ*, 593, L93
- Ertan, Ü., & Çalışkan, Ş. 2006, *ApJ*, 649, L87
- Ertan, Ü., & Cheng, K. S. 2004, *ApJ*, 605, 840
- Ertan, Ü., Ekşi, K. Y., Erkut, M. H., & Alpar, M. A. 2009, *ApJ*, 702, 1309
- Ertan, Ü., & Erkut, M. H. 2008, *ApJ*, 673, 1062
- Ertan, Ü., Erkut, M. H., Ekşi, K. Y., & Alpar, M. A. 2007, *ApJ*, 657, 441
- Ertan, Ü., Göğüş, E., & Alpar, M. A. 2006, *ApJ*, 640, 435
- Esposito, P., Burgay, M., Possenti, A., et al. 2009, *MNRAS*, 399, L44
- Frank, J., King, A. R., & Raine, D. J. 2002, *Accretion Power in Astrophysics* (3rd ed.; Cambridge: Cambridge Univ. Press)
- Gotthelf, E. V., & Halpern, J. P. 2007, *Ap&SS*, 308, 79
- Gotthelf, E. V., Halpern, J. P., Buxton, M., & Bailyn, C. 2004, *ApJ*, 605, 368
- Ibrahim, A. I., Markwardt, C. B., Swank, J. H., et al. 2004, *ApJ*, 609, 21
- Israel, G. L., Campana, S., Dall’Osso, S., et al. 2007, *ApJ*, 664, 448
- Kouveliotou, C., Eichler, D., Woods, P. M., et al. 2003, *ApJ*, 596, L79
- Krimm, H., Barthelmy, S., Campana, S., et al. 2006, *ATel*, 894
- Kumar, H. S., Ibrahim, A. I., & Harb, S. S. 2010, *ApJ*, 716, 97
- Lasota, J.-P. 2001, *New Astron. Rev.*, 45, 449
- Lazaridis, K., Jessner, A., Kramer, M., et al. 2008, *MNRAS*, 390, 839
- Mereghetti, S. 2008, *A&AR*, 15, 225
- Mereghetti, S., Esposito, P., Tiengo, A., et al. 2006, *A&A*, 450, 759
- Mereghetti, S., Tiengo, A., Esposito, P., et al. 2009, arXiv:0908.0414
- Muno, M. P., Gaensler, B. M., Clark, J. S., et al. 2007, *MNRAS*, 378, L44
- Nakagawa, Y. E., Makishima, K., & Enoto, T. 2011, *PASJ*, 63, S813
- Page, D., Geppert, U., & Weber, F. 2006, *Nucl. Phys. A*, 777, 497
- Palmer, D., Esposito, P., Barthelmy, S., et al. 2008, *ATel*, 1548
- Rea, N., Esposito, P., Turolla, R., et al. 2010, *Science*, 330, 944
- Rea, N., Israel, G. L., Turolla, R., et al. 2009, *MNRAS*, 396, 2419
- Savchenko, V., Neronov, A., Beckmann, V., Produit, N., & Walter, R. 2010, *A&A*, 510, 77
- Shakura, N. I., & Sunyaev, R. A. 1973, *A&A*, 24, 337
- Tam, C. R., Kaspi, V. M., Gaensler, B. M., & Gotthelf, E. V. 2006, *ApJ*, 652, 528
- Trümper, J. E., Zezas, A., Ertan, Ü., & Kylafis, N. D. 2010, *A&A*, 518, 46
- Tuchman, Y., Mineshige, S., & Wheeler, J. C. 1990, *ApJ*, 359, 164
- Wang, Z., Chakrabarty, D., & Kaplan, D. L. 2006, *Nature*, 440, 772
- Woods, P. M., Kaspi, V. M., Gavriil, F. P., & Airhart, C. 2011, *ApJ*, 726, 37